Автоматизовані системи управління та прилади автоматики. 2025. № 4 (187)

UDC 621.396 **DOI:** https://doi.org/10.30837/0135-1710.2025.187.299

D. Kovalchuk, O. Zhyla

MEASUREMENT GEOMETRY, SIGNAL MODELS AND ALGORITHMS FOR RADIO IMAGE RECOVERY IN SYNTHESIZED APERTURE RADARS USING CONTINUOUS LFM SIGNALS

This article analyzes the methods of forming radar images on the surface formed by SAR with a continuous LFM probing signal. It is of interest to determine the main algorithmic operations performed on the "raw" data after their registration in the receivers. The geometry of measurements, the sounding signal and the features of the formation of "raw" data that will determine further processing will be considered. To compare the quality of work of different algorithms, a simulation model of the formation of radar images in RSA with the processing of continuous LFM signals has been developed. **The aim of the work** is to create a universal geometric basis for building effective measurement schemes and signal processing algorithms in radio engineering systems. **The research tasks** include: 1) formalization of the problem of determining coordinates based on the results of direction-finding measurements; 2) construction of a mathematical model of the mutual location of objects in three-dimensional space; 3) determination of the influence of geometric factors on the measurement accuracy; 4) analysis of single and multiple observation options. **The results obtained** allow establishing an analytical relationship between the measurement parameters and the configuration of the spatial scene, which ensures an increase in the accuracy of coordinate determination. **Field of application**: the results can be used to increase the efficiency of navigation, reconnaissance and monitoring systems, as well as in the tasks of tracking moving objects and building situational awareness systems.

Keywords: measurement geometry; direction finding; coordinate determination; three-dimensional model; radio measurement system.

Relevance

In today's environment of active development of unmanned aerial vehicles, monitoring and reconnaissance systems, there is a growing need for accurate determination of the coordinates and trajectories of radio emission sources. Reliable positioning is critical to ensuring the autonomy and effectiveness of such systems. Most measurement tasks require consideration of the spatial geometry of the scene, but existing approaches often simplify the model to two dimensions, which limits accuracy. Building a three-dimensional geometric model allows for adequate consideration of the influence of the location of receivers and signal sources. This, in turn, improves data processing algorithms and reduces coordinate determination errors.

The analysis of the influence of space configuration on measurement results during multiple observations is particularly relevant. Understanding geometric constraints allows for the rational placement of sensors and optimization of observation trajectories. The creation of a universal spatial model is an important prerequisite for the construction of high-precision radio measurement systems.

Therefore, the study of measurement geometry is of great importance for the development of modern radio engineering and navigation technologies.

Measurement geometry in the formation of radar images in the SAR from an aircraft

To illustrate the principle of forming an "artificial" aperture, we will use the geometry shown in Fig. 1 [1].

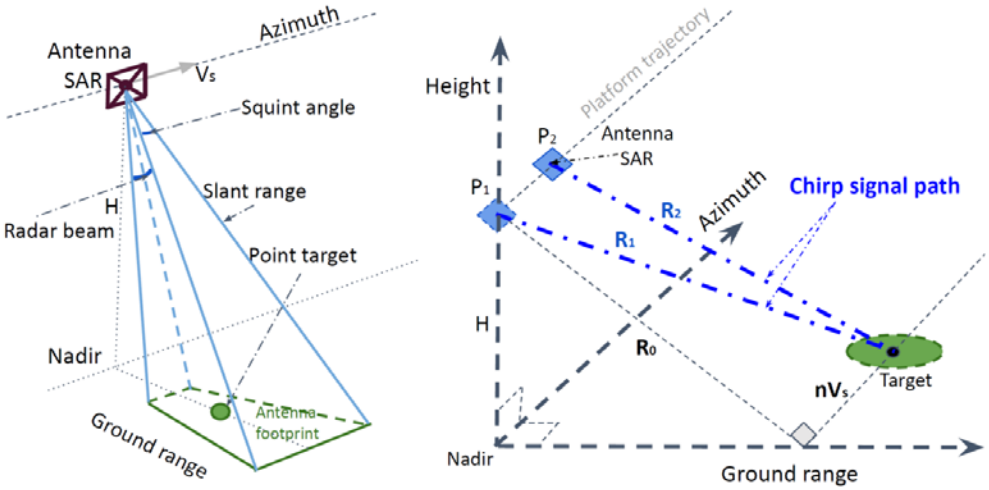

a b

Fig. 1. Geometry of surface scanning by radar implementing the antenna aperture synthesis algorithm: *a* – spatial position of the beam of a non-synthesized antenna; *b* – distance traveled by the signal during the movement of the carrier (taken from [1])

The idea of forming a synthesized aperture is the same for both pulsed and continuous wave radars. First, electromagnetic waves are emitted from an onboard antenna mounted on a moving platform (see Fig. 1 Antenna SAR) in the direction of the surface within the non-synthesized directional pattern, over a wide range of angles. The platform moves in a straight line at a speed V_s along a coordinate conventionally called Azimuth. The coordinate is called Azimuth because the synthesis of the antenna reduces the width of the directional pattern at the azimuth angle in a spherical coordinate system.

Thus, traditionally in the literature, SAR resolution or image characteristics are associated with the conventional azimuth coordinate. At the same time, all radar images are converted to Cartesian surface coordinates with units of measurement in meters. Another coordinate that plays an important role in measurements is the ground range (in Fig. 1 Ground range).

Ground range is converted from slant range (Fig. 1 Slant range) within the beam width of the physical antenna's directional pattern. The beam width is perpendicular to the flight path (Fig. 1 Radar beam) and determines the width of the viewing range along the ground range coordinate. In practice, the wider the viewing range, the faster the radio image of a given surface area is formed.

The size of the radio image pixel along the ground range coordinate is determined by the radar's resolution along the slant range. At oblique range, the resolution determines how many areas can be observed separately along the entire signal propagation path. Each area has

a constant value at oblique range, but when converted to ground range, the sizes of the areas change according to the formula

$$\Delta R_{Ground\ range} = \frac{\Delta R_{Slant\ range}}{\sin\theta}, \quad (1)$$

where $\Delta R_{Slant\ range}$ – resolution of the radio system in terms of slant range, θ – angle of observation of each point on the surface, $\Delta R_{Ground\ range}$ – resolution of the radio system in terms of ground range. The geometry of recalculating the areas of separate observation of objects on the surface is shown in Fig. 2.

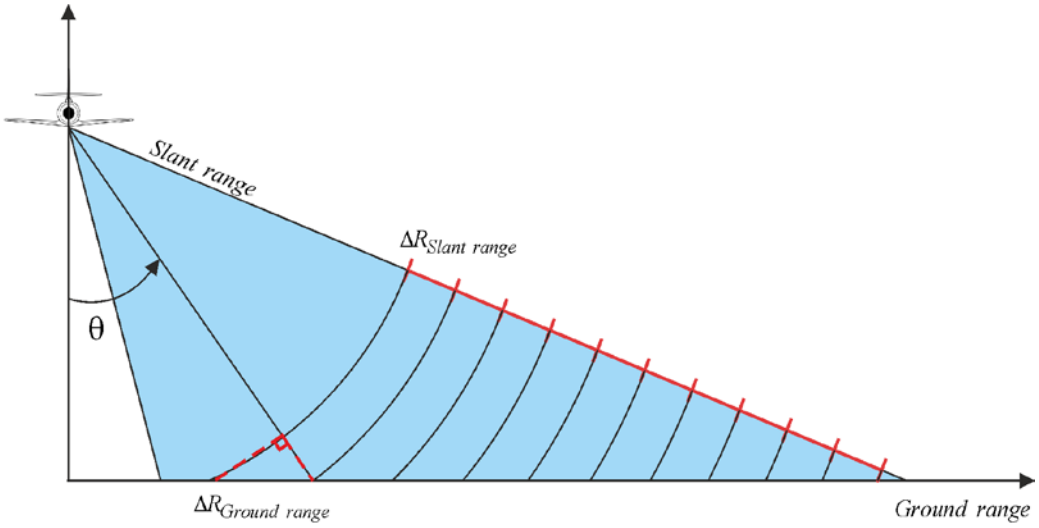

Fig. 2. Geometric transformations of resolution at slant range into resolution at ground range

The resolution in ground range for all types of probing signals is inversely proportional to their spectral width, therefore, along this coordinate, the main attention is paid to signal processing in time and within a certain modulation period [2–4]. Resolution along the other coordinate, azimuth, is determined by spatially-temporally coherent processing of complex envelope reflected signals accumulated during motion [2–4].

Fig. 1, *b* shows the process of signal emission from point P_1 and its reception at point P_2. The observation of the object (in Fig. 1, *a* Point target, in Fig. 1, *b* Target) occurs over a certain period of time, while the directional pattern, having a certain width along the flight path (in Fig. 1, *a* Squint angle), irradiates it.

The observation time at a fixed carrier speed or the interval of spatial accumulation of reflected signals determines the size of the synthesized aperture. The azimuth resolution is inversely proportional to the size of the synthesized aperture in the azimuth coordinate [2–4]. The azimuth resolution in angular coordinates at a known height and elevation angle or at a known slant range is converted into the resolution in spatial coordinates on the surface.

Thus, we have considered the geometry of measurements in SAR and determined the main values that affect the resolution of radar images.

A probing signal with linear frequency modulation looks like this [5]:

$$\dot{s}_t(t) = \exp\left\{ j\left(2\pi f_0 t + \pi k_r t^2\right)\right\}, \quad (2)$$

where $f_0 = c/\lambda$ is the carrier frequency of the probing signal, c is the speed of radio wave propagation, λ is the wavelength, $\pi k_r t^2$ is the quadratic phase shift inherent in the LFM signal, $k_r = \Delta f / t_p$ the rate of frequency change by an amount Df over the modulation period t_p.

In expression (2), a dot is placed above the probe signal designation, emphasizing that the signal model is presented in complex form. This approach is a mathematical simplification of all subsequent calculations. The physical signal emitted by the antenna cannot be complex and is described by the harmonic signal model as follows:

$$s_t(t) = A\cos\left(2\pi f_0 t + \pi k_r t^2\right), \quad (3)$$

where A is the amplitude of the harmonic oscillation. The following mathematical operations can be performed on expression (3):

$$\begin{aligned} s_t(t) &= A\cos\left(2\pi f_0 t + \pi k_r t^2\right) = \\ &= A\,\mathrm{Re}\left\{\exp\left(2\pi f_0 t + \pi k_r t^2\right)\right\}. \end{aligned}, \quad (4)$$

Assuming that the amplitude of the probing signal is equal to 1, in further calculations we move on to complex signals, omitting the operator $\mathrm{Re}\{\cdot\}$ and denoting $s_t(t)$ with a dot above. The received signal reflected from the surface has the form [5]

$$\dot{s}_r(t) = \exp\left\{ j\left(2\pi f_0 \left(t-\Delta t\right) + \pi k_r \left(t-\Delta t\right)^2\right)\right\}, \quad (5)$$

where $\Delta t = \left(R_1(n) + R_2(n)\right)/c$ – is the signal delay time during propagation, distances $R_1(n)$ and $R_2(n)$ are shown in Fig. 1, *b*. The variable n in distances is referred to in the literature as slow time, azimuth time, or azimuth coordinate of the radar image.

As a result of the carrier's movement, the received signal will have a Doppler frequency shift, which changes the initial carrier frequency by an amount $\alpha = c^2/\left(c^2 - V_s^2\right)$. Taking into account the formula for range [1]:

$$R_1(n) = \sqrt{R_0^2 + \left(V_s n\right)^2}, \quad (6)$$

we obtain the delay time

$$\Delta t = 2\alpha\left(R_1(n)/c + \left(V_s/c\right)^2 n\right). \quad (7)$$

In (6), R_0 – the range to the surface point at an angle of 90 degrees to the flight path.

According to the classical theory of optimal signal processing [7, 8], received signals must be processed in a matched filter or undergo correlation processing in a correlation integral. In radars with continuous LFM signal processing, the impulse response of the matched filter repeats the probing signal. Physical devices for implementing such processing include

a linear receiver path with a set of filters (input circuits, high-frequency filter), mixer, intermediate frequency filter, mixer for transfer to the zero-frequency region, low-frequency filter, low-frequency amplifier [8–10]. At the output of the matched filter after multiplication (5) and (2), we obtain

$$\dot{s}_{dc}(t) = \dot{s}_t(t)\dot{s}_r^*(t) = \\ = \exp\left\{ j\left(2\pi f_0 t + \pi k_r t^2\right)\right\} \exp\left\{ -j\left(\begin{array}{l} 2\pi f_0 (t-\Delta t) + \\ +\pi k_r (t-\Delta t)^2 \end{array} \right)\right\} = \\ = \exp\left\{ j\left(2\pi f_0 \Delta t + 2\pi k_r t \Delta t - \pi k_r \Delta t^2\right)\right\}, \quad (8)$$

where $(\cdot)^*$ – complex conjugation sign.

The resulting expression (8) can be discretized and further processed by a computer. This expression can also be used to test various algorithms for restoring radar images and focusing radio systems. Let us consider these algorithms in more detail.

Algorithms for restoring radar images in SAR with continuous LFM signal processing

Based on the analysis of the literature and formulas (1)–(8) presented, it can be stated that the radar image is represented in the coordinates of "fast" time *t* along the ground range and "slow" time *n* along the azimuth [1]. However, this representation is conditional, since in essence it only shows that spatial-temporal signal processing is necessary to form a radar image.

In the literature, such processing of received signals is also called two-dimensional and, in general, can be performed in four variations: 1) processing in time by ground range and processing in time by azimuth, 2) processing in the spectrum by ground range and processing in time by azimuth, 3) processing in time by ground range and processing in spectrum by azimuth, 4) spectral processing of signals by ground range and azimuth.

These four approaches and modifications of each of the time or spectrum processing methods have led to the development of a large number of algorithms for forming radio images based on the results of receiving so-called “raw” data in expression (8). Let us consider the main ones.

Omega-K algorithm (ωKA)

This algorithm accepts the assumption that $\Delta t^2 \to 0$ and phase shift $\pi k_r \Delta t^2$ does not carry useful information [5, 11]. In this case, the expression for "raw" data will look like this:

$$\dot{s}_0(t,n) = \exp\left\{ j\left(2\pi f_0 \Delta t + 2\pi k_r t \Delta t\right)\right\}. \quad (9)$$

The first mathematical operation on (9) is the Fourier transform by coordinate t:

$$\dot{S}(f_t, n) = \int_{-t_0/2}^{t_0/2} \dot{s}_0(t,n) \cdot \exp\left(-j2\pi f_t t\right) dt, \quad (10)$$

where t_0 – observation time of received signals.

Next, we determine the Fourier transform by azimuth

$$\dot{S}(f_t, f_n) = \int_{-\infty}^{\infty} \dot{S}(f_t, n) \cdot \exp(-j2\pi f_n n)\, dn. \quad (11)$$

After calculating the Fourier transform in two coordinates, we obtain "raw" data for further processing in the spectral plane:

$$\dot{S}(f_t, f_n) = t_0 \mathrm{sinc}\left(\pi t_0 (f_t - k_r \Delta t)\right) \exp\left(j\varphi(f_t, f_n)\right), \quad (12)$$

where $\varphi(f_t, f_n) = \frac{4\pi\alpha R_0}{c}\sqrt{(f_0 + f_t)^2 - \left(cf_n/(2\alpha V_s)\right)^2}$ – frequencies by "fast" time coordinate t, f_n – frequencies by the "slow" time coordinate n.

The algorithm for processing "raw" data (12) according to the Omega-K algorithm is shown in Fig. 3.

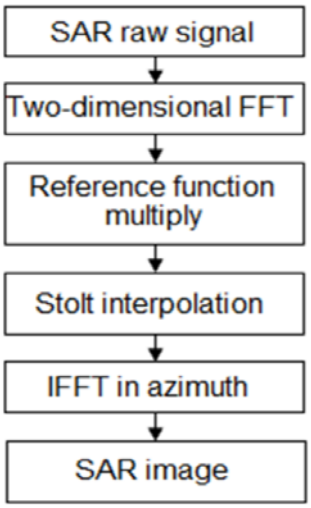

Fig. 3. Omega-K algorithm for processing "raw" data in SAR with continuous LFM signals (taken from [5])

After converting the received signals into spectral form, the resulting expression (12) is multiplied by the reference function

$$\dot{H}_{ref}(f_t, f_n) = \exp\left(-j\varphi_{ref}(f_t, f_n)\right), \quad (13)$$

where

$$\varphi_{ref}(f_t, f_n) = 4\pi\alpha R_{ref} \times \times\sqrt{(f_0 + f_t)^2 - \left(cf_n/(2\alpha V_s)\right)^2}\Big/c. \quad (14)$$

After multiplication, the phase will look like this:

$$\varphi_{RFM}(f_t, f_n) = 4\pi\alpha\left(R_0 - R_{ref}\right)\times \times\sqrt{(f_0 + f_t)^2 - \left(cf_n/(2\alpha V_s)\right)^2}\Big/c, \quad (15)$$

The next mathematical operation consists in interpolating data using the Stolt method [12–14].

This interpolation is performed in connection with the "migration" of the range to a separate point on the surface during the straight-line motion of the carrier.

The effect of range migration is shown in Fig. 4.

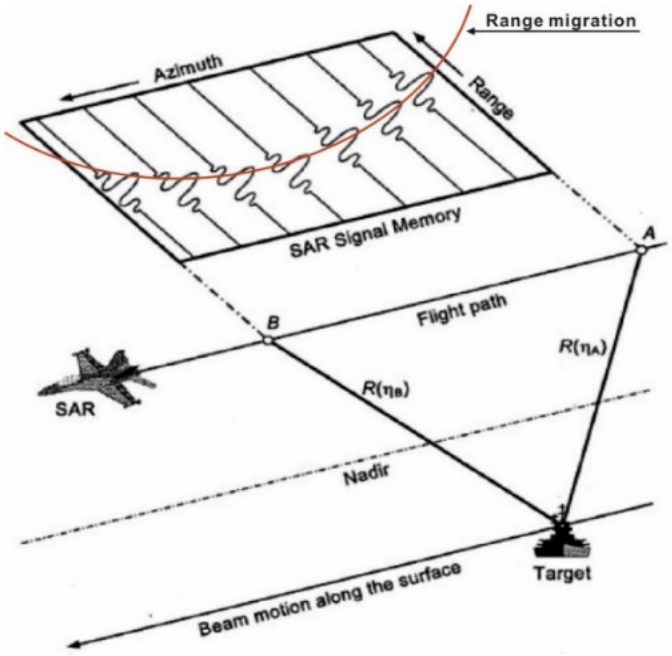

Fig. 4. Range migration to a point target in SAR ([1])

The range migration effect also manifests itself in the spectrum of received signals and leads to defocusing of radar images. The principle of data interpolation using the Stolt method is demonstrated in Fig. 5.

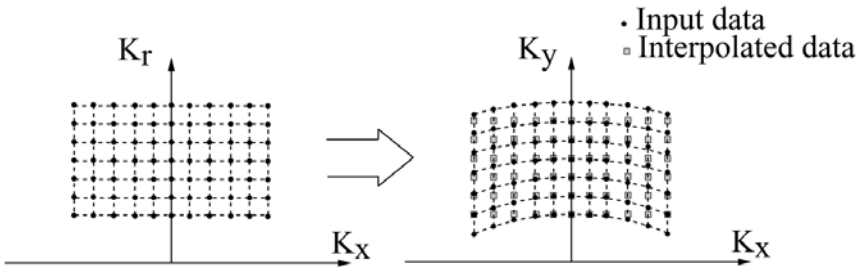

Fig. 5. Data interpolation using the Stolt method (taken from [15])

The essence of the presented interpolation is to replace the law of variation f_t from linear to nonlinear in such a way that the following equality occurs in expression (15):

$$\sqrt{\left(f_0 + f_t\right)^2 - \left(cf_n/\left(2\alpha V_s\right)\right)^2} = f_0 + f_t'. \qquad (16)$$

In other words, it is necessary to replace f_t with a new variable f_t' to compensate for the "migration" of the distance along the coordinate f_t. Many works [1–10] are devoted to the issue

of interpolation using the Stolt method, most of which conclude that the new variable should be calculated as follows:

$$f_t' = \sqrt{\left(f_0 + f_t\right)^2 - \left(\frac{cf_n}{2\alpha V_s}\right)^2} - f_0\sqrt{1 - \left(\frac{cf_n}{2\alpha V_s f_0}\right)^2}\,. \tag{17}$$

The phase after interpolation will look like this

$$\varphi_{RFM}\left(f_t, f_n\right) = 4\pi\alpha\left(R_0 - R_{ref}\right)\cdot\left(f_0 + f_t'\right)/c\,. \tag{18}$$

The last algorithmic operation consists in calculating the inverse Fourier transform by azimuth. The result is a radar image of the surface formed by SAR with processing of continuous LFM signals. It should be noted that when implementing the Omega-K algorithm in pulse SAR, at the last stage it is necessary to calculate a two-dimensional Fourier transform in azimuth and range. A feature of processing in SAR with continuous LFM signals is the availability of information about the surface characteristics in each spectral component.

Modified Omega-K algorithm (ωKA-M)

The block diagram of the ωKA-M algorithm [16] is shown in Fig. 6.

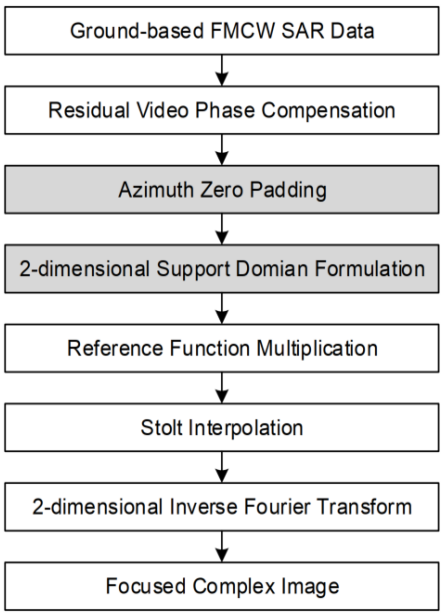

Fig. 6. Modified Omega-K algorithm for processing raw data in SAR with continuous LFM signals ([16])

Unlike the previous algorithm, instead of assuming that the phase component $\pi k_r \Delta t^2$ is insignificant, in this algorithm, the first operation is to compensate for it by calculating the forward Fourier transform in range, multiplying by the function

$$\dot{S}_{RVP}\left(f_t\right) = \exp\left(-j\left(\pi f^2 / k_r\right)\right), \tag{19}$$

and calculating the inverse Fourier transform in range.

The next operation in the block diagram in Fig. 6 is to supplement the "raw" data with zeros along the azimuth coordinate. This method was developed for a ground station with aperture synthesis moving on rails. The research in this work is devoted to the formation of radio images from an aircraft, where data is constantly fed into the processor during movement and, in this case, there is no need to supplement with zeros.

The main difference between the modified algorithm is the formation of two-dimensional data at the stage that the authors [16] called 2-dimensional Support Domain Formulation. To explain the essence of this operation, let us write down another representation of "raw" data

$$\dot{s}_0(t,x)=\exp\left\{j\left(2\pi f_0\frac{2R(x)}{c}+2\pi k_r t\frac{2R(x)}{c}\right)\right\}\times \\ \times\exp\left\{j\left(4\pi k_r/c^2\right)R^2(x)\right\}, \tag{20}$$

where x the analogue of "slow" time n, is just represented in more physical quantities – surface coordinates, $x=V_s\Delta t+x_n$, $x_n=V_s nT_p$ – discrete positions of the SAR carrier, n – discretization period number, T_p – modulation period of the probing LFM signal.

For further processing, a variable $k_r t=f_t$, frequency is introduced for the range coordinate, and the range is written as follows

$$R(x)=\sqrt{R_0^2+(x_0-x)^2}\,. \tag{21}$$

Substituting the expressions given in (20) and performing RVP compensation, we obtain the result of the first stage of two-dimensional data formation

$$\dot{S}(f_t,x_n)=\exp\left\{j\left((4\pi/c)\cdot(f_0+f_t)\times \right.\right. \\ \left.\left.\times\sqrt{R_0^2+\left(x_n-x_0+V_s f_t/k_r\right)^2}\right)\right\}. \tag{22}$$

The next step is to calculate the Fourier transform by azimuth.

$$\dot{S}(f_t,x_n,f_x)=\int_{-\infty}^{\infty}\dot{S}(f_t,x_n)\cdot\exp\{-j2\pi f_x x_n\}\,dx_n\,, \tag{23}$$

where f_x – frequency by azimuth coordinate. The phase in expression (23) has the following form:

$$\Phi(f_t,x_n,f_x)=-(4\pi/c)\cdot(f_0+f_t)\times \\ \times\sqrt{R_0^2+\left(x-x_0+V_s f_t/k_r\right)^2}-2\pi f_x x_n. \tag{24}$$

Using the principle of the stationary phase

$$\frac{d\Phi(f_t,x_n,f_x)}{dx_n}=0\,,$$

we obtain an expression for the azimuth coordinates

$$x_n=-\frac{cR_0 f_x}{\sqrt{4(f_0+f_t)^2-c^2 f_x^2}}+x_0-\frac{V_s f_t}{k_r}. \tag{25}$$

Substituting (25) into (24), we obtain a two-dimensional representation of data in the spectrum for further processing using already known algorithmic operations

$$\dot{S}\left(f_t, f_x\right) = \exp\left\{\begin{array}{c} -\dfrac{4\pi R_0}{c}\sqrt{\left(f_0 + f_t\right)^2 + c^2 f_x^2/4} - \\ -2\pi f_x x_0 + \left(2\pi V_s/k_r\right)\cdot f_t f_x \end{array}\right\}. \quad (26)$$

Frequency Scaling Algorithm (FSA or CSA) and Range-Doppler algorithm (RDA)

Complete information on the implementation of the FSA algorithm is presented in [17–19], and the block diagram is shown in Fig. 7, *a*. The RDA algorithm is described in detail in [17, 20, 21] and demonstrated in Fig. 7, *b*. From the analysis of the main operations, it follows that FSA is supplemented with new RDA operations.

In this case, let us consider in detail all the main operations using the frequency scaling method. First of all, it should be noted that the "raw" data is represented as $s(t,\eta)$ and fully corresponds to expression (9), only instead of the variable for "slow" time n, η is used.

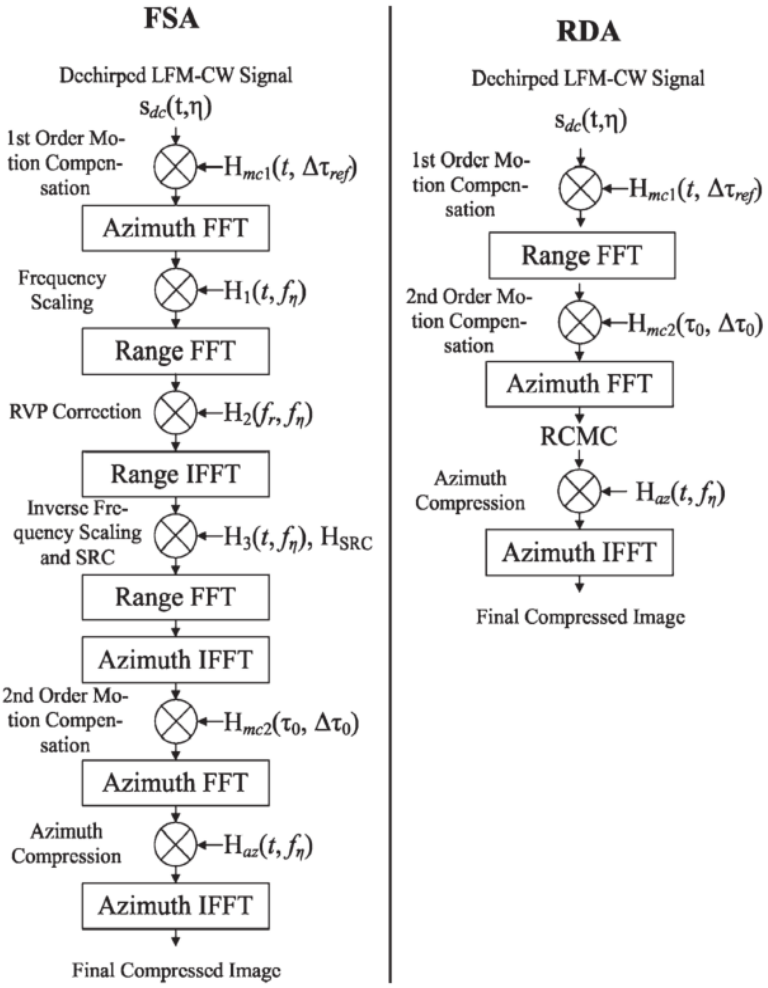

a b

Fig. 7. Methods for processing "raw" data in SAR with continuous LFM signals: *a* – frequency scaling method; *b* – Range-Doppler method (taken from [17])

The first operation on the received signals is to compensate for the carrier's own motion, which consists of multiplying the received signals by the function

$$H_{mc1}\left(t,\Delta\tau_{ref}\right)=\exp\left\{-j\left(2\pi f_0\Delta\tau_{ref}+\right.\right.$$
$$\left.\left.+2\pi k_r t\Delta\tau_{ref}-\pi k_r\left(2\eta\Delta\tau_{ref}-\tau_{ref}^2\right)\right)\right\}, \quad (27)$$

where $\Delta\tau_{ref}=2\Delta R_{ref}/c$, $\Delta R_{ref}=R_{actual}-R_{ideal}$, R_{actual} – sloped range from the carrier to the point target, taking into account known deviations of the platform from the ideal trajectory; R_{ideal} – the ideal trajectory of the platform for the same position of the point target.

The next stage of processing according to the FSA and RDA algorithms is the calculation of the Fourier transform by azimuth and frequency scaling of data together with the elimination of Doppler frequency shift, which consists in multiplying the preliminary result by the function

$$H_1\left(t,f_\eta\right)=$$
$$=\exp\left\{-j\left[2\pi f_\eta t+\pi k_r t^2\left(1-D\left(f_\eta,V_s\right)\right)\right]\right\}, \quad (28)$$

where $D\left(f_\eta,V_s\right)=\sqrt{1-\lambda^2 f_\eta^2/\left(4V_s^2\right)}$ – coefficient determining the degree of range migration.

After frequency scaling, a Fourier transform is performed in the range and in the frequency domain, and the constant phase with a quadratic ramp is compensated for in the range, as was done in the ωKA-M algorithm.

Compensation for the excess phase is performed by multiplying the data by the function

$$H_2\left(f_r,f_\eta\right)=\exp\left\{-j\left(\pi f_r^2/\left(k_r D\left(f_\eta,V_s\right)\right)\right)\right\}. \quad (29)$$

After performing the inverse Fourier transform in range, inverse frequency scaling is performed by multiplying by the function

$$H_3\left(t,f_\eta\right)=$$
$$=\exp\left\{-j\pi k_r t^2\left[D^2\left(f_\eta,V_s\right)-D\left(f_\eta,V_s\right)\right]\right\}. \quad (30)$$

At this stage, secondary range correction and phase shift compensation for range are also introduced, as described in detail in [18].

Next, the signal is sequentially transformed into the spectral plane by range, and an inverse Fourier transform is applied by azimuth. In the resulting two-dimensional signal, range migration is secondarily compensated by multiplying the data by the function

$$H_{mc2}\left(\tau_0,\Delta\tau_0\right)=\exp\left\{-j\left(2\pi f_0\Delta\tau_0+\right.\right.$$
$$+2\pi k_r\tau_0\Delta\tau_0-\pi k_r\Delta\tau_0^2+2\pi f_0\Delta\tau_{ref}-.$$
$$\left.\left.-2\pi k_r\tau_{ref}\Delta\tau_{ref}+\pi k_r\Delta\tau_{ref}^2\right)\right\}, \quad (31)$$

where $\tau_0=2R_0/c$, $\Delta\tau_0=2\Delta R_0/c$, $\tau_{ref}=2R_{ref}/c$, $\Delta\tau_{ref}=2\Delta R_{ref}/c$.

The following operations are known from previous methods: calculation of Fourier transform by azimuth, data compression by azimuth, calculation of inverse Fourier transform by azimuth.

The difference between these operations lies only in their names; their essence remains the same. Azimuth data compression is the same operation as multiplication by a reference function in the ωKA and ωKA-M algorithms.

Modified frequency scaling method (FSA-M)

This algorithm is an extension of the FSA algorithm [22, 23], which is shown in Fig. 8

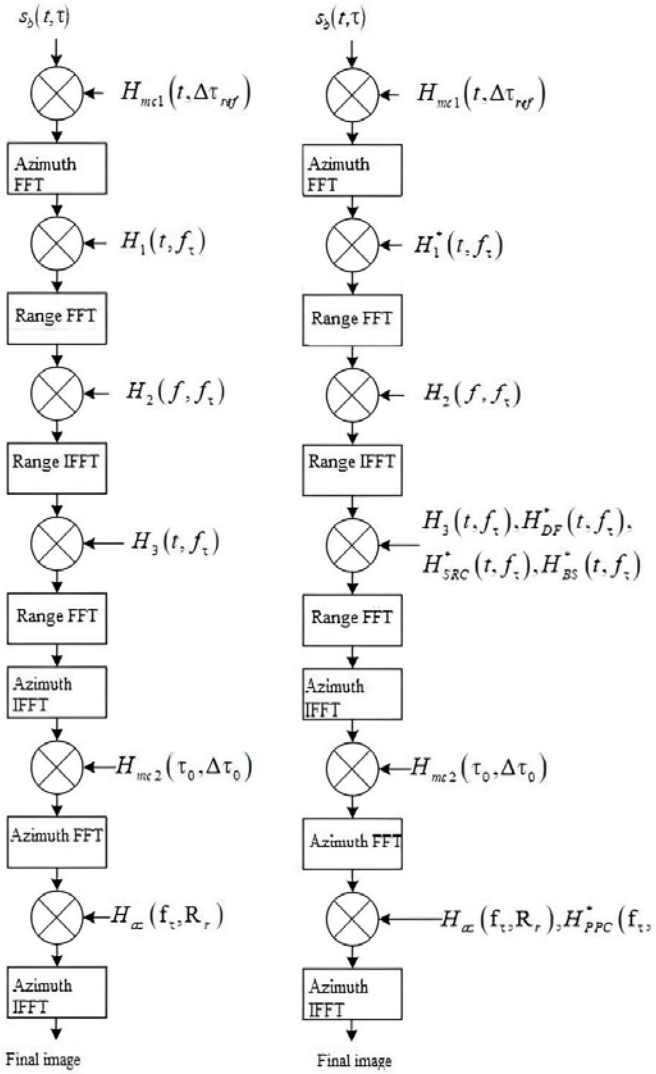

a b

Fig. 8. Methods for processing "raw" data in SAR with continuous LFM signals: *a* – frequency scaling method; *b* – modified frequency scaling method

If we disregard the forward and inverse Fourier transforms in range and azimuth and the carrier motion compensation operations, the key differences between the algorithms are as follows.

The frequency scaling function in the modified algorithm takes the form, instead of (28),

$$H_1^*\left(t,\, f_\eta\right)=\exp\left\{-j\pi k_r t^2\left(1-D\left(f_\eta,V_s\right)\right)\right\}. \tag{32}$$

In the modified algorithm, after the inverse Fourier transform, the data is multiplied by three more functions that perform:

1) Doppler shift correction

$$H_{DF}^*\left(t,\, f_\eta\right)=\exp\left\{-j2\pi f_\eta D\left(f_\eta,V_s\right)t\right\}, \tag{33}$$

2) second-order range compression

$$H_{SRC}^*\left(t,\, f_\eta\right)=\exp\left\{\begin{array}{c}-j\dfrac{2\pi R_{ref}k_r^2\lambda}{c^2}\dfrac{D^2\left(f_\eta,V_s\right)-1}{D^3\left(f_\eta,V_s\right)}\times\\ \times\left(D\left(f_\eta,V_s\right)t-2R_{ref}/c\right)^2\end{array}\right\}\times$$

$$\times\exp\left\{\begin{array}{c}-j\dfrac{2\pi R_{ref}k_r^3\lambda^3}{c^3}\dfrac{D^2\left(f_\eta,V_s\right)-1}{D^5\left(f_\eta,V_s\right)}\times\\ \times\left(D\left(f_\eta,V_s\right)t-2R_{ref}/c\right)^3\end{array}\right\}, \tag{34}$$

3) group phase shift compensation

$$H_{BS}^*\left(t,\, f_\eta\right)=$$

$$=\exp\left\{\begin{array}{c}-j\dfrac{4\pi k_r}{c}R_{ref}\left(\dfrac{1}{D(f_\eta,V_s)}-1\right)\times\\ \times\left(D\left(f_\eta,V_s\right)t-2R_{ref}/c\right)\end{array}\right\}. \tag{35}$$

At the final stage, when compressing data by azimuth, multiplication by the phase preservation function is additionally introduced.

$$H_{PPC}^*\left(f_r,\, f_\eta\right)=\exp\left\{j\frac{4\pi R_{ref}}{c}\frac{f_r}{D\left(f_\eta,V_s\right)}\right\}. \tag{36}$$

The presented modified algorithm is similar to the existing FSA, but has the advantage of taking into account the compensation of carrier motion during emission in signal processing.

The classic FSA was borrowed from the algorithms of pulse SAR, where the emission time is significantly less than the observation time of the reflected signals. In SAR with continuous LFM signal processing, the radiation time is significant and the carrier motion must be taken into account in this case.

Conclusions

The article considers a generalized approach to constructing spatial models that describe the process of measuring the coordinates of radio emission sources. Geometric schemes are proposed that allow formalizing the mutual location of the source and receiver in three-dimensional space. Functional dependencies between measurement parameters and scene configuration are established. It is shown that geometric factors significantly affect the accuracy

of coordinate determination. Particular attention is paid to multiple observation options that reduce ambiguity and increase the reliability of results. The analysis confirms the feasibility of using three-dimensional models in direction finding and navigation tasks. The results obtained can serve as a basis for the development of new signal processing algorithms in radio measurement systems.

The proposed approach opens up opportunities for improving sensor placement and trajectory planning. The research has both theoretical and practical significance. Further work may be directed toward the practical implementation of simulation models and testing their effectiveness in real-world conditions.

References

1. Jancco-Chara, J., Palomino-Quispe, F., Coaquira-Castillo, R. J., Herrera-Levano, J. C., Florez, R. (2024), "Doppler Factor in the Omega-k Algorithm for Pulsed and Continuous Wave Synthetic Aperture Radar Raw Data Processing", *Applied Sciences*, Vol. 14, P. 320. DOI: https://doi.org/10.3390/app14010320
2. Ulaby, F. T., Moore, R. K., Fung, A. K. (1986), *Microwave Remote Sensing: Active and Passive*, Vol. II, ARTECH House, Norwood, Massachusetts, P. 583–595.
3. Curlander, J. C., McDonough, R. N. (1991), *Synthetic Aperture Radar: Systems and Signal Processing*, John Wiley & Sons, New York.
4. Elachi, C. (1988), *Spaceborne Radar Remote Sensing: Applications and Techniques*, IEEE Press, New York.
5. Chara, J. J., Palomino-Quispe, F., Coaquira-Castillo, R. J., Clemente-Arenas, M. (2020), "Omega-k Algorithm Implementation for Linear Frequency Modulated-Continuous Wave SAR Signal Processing", *IEEE INTERCON 2020*, Lima, Peru, P. 1–4. DOI: https://doi.org/10.1109/INTERCON50315.2020.9220195
6. Volosyuk, V., Zhyla, S. (2022), "Statistical Theory of Optimal Functionally Deterministic Signals Processing in Multichannel Aerospace Imaging Radar Systems", *Computation*, Vol. 10, P. 213. DOI: https://doi.org/10.3390/computation10120213
7. Volosyuk, V., Zhyla, S. (2022), "Statistical Theory of Optimal Stochastic Signals Processing in Multichannel Aerospace Imaging Radar Systems", *Computation*, Vol. 10, P. 224. DOI: https://doi.org/10.3390/computation10120224
8. Stringham, C., Long, D. G., Wicks, B., Ramsey, G. (2011), "Digital Receiver Design for an Offset IF LFM-CW SAR", *IEEE RadarCon 2011*, Kansas City, USA, P. 960–964. DOI: 10.1109/RADAR.2011.5960678
9. Aguasca, A., Acevo-Herrera, R., Broquetas, A., Mallorqui, J. J., Fabregas, X. (2013), "ARBRES: Light-Weight CW/FM SAR Sensors for Small UAVs", *Sensors*, Vol. 13, P. 3204–3216. DOI: https://doi.org/10.3390/s130303204
10. Mencia-Oliva, B., Grajal, J., Yeste-Ojeda, O. A., Rubio-Cidre, G., Badolato, A. (2013), "Low-Cost CW-LFM Radar Sensor at 100 GHz", *IEEE Transactions on Microwave Theory and Techniques*, Vol. 61, No. 2, P. 986–998. DOI: https://doi.org/10.1109/TMTT.2012.2235457
11. Cumming, I. G., Neo, Y. L., Wong, F. H. (2003), "Interpretations of the Omega-K Algorithm and Comparisons with Other Algorithms", *IGARSS 2003*, Toulouse, France, P. 1455–1458. DOI: https://doi.org/10.1109/IGARSS.2003.1294142

12. Stolt, R. H. (1978), "Migration by Transform", *Geophysics*, Vol. 43, No. 1, P. 23–48.
13. Chun, J. H., Jacowitz, C. A. (1981), "Fundamentals of Frequency Domain Migration", *Geophysics*, Vol. 46, P. 717–733.
14. Cafforio, C., Prati, C., Rocca, F. (1991), "SAR Data Focusing Using Seismic Migration Techniques", *IEEE Transactions on Aerospace and Electronic Systems*, Vol. 27, No. 2, P. 194–207.
15. Subiza, B., Gimeno-Nieves, E., Lopez-Sanchez, J. M., Fortuny-Guasch, J. (2003), "An Approach to SAR Imaging by Means of Non-Uniform FFTs", *IGARSS 2003*, Toulouse, France, Vol. 6, P. 4089–4091. DOI: https://doi.org/10.1109/IGARSS.2003.1295371
16. Guo, S., Dong, X. (2016), "Modified Omega-K Algorithm for Ground-Based FMCW SAR Imaging", *ICSP 2016*, Chengdu, China, P. 1647–1650. DOI: https://doi.org/10.1109/ICSP.2016.7878107
17. Zaugg, E. C., Long, D. G. (2008), "Theory and Application of Motion Compensation for LFM-CW SAR", *IEEE Transactions on Geoscience and Remote Sensing*, Vol. 46, No. 10, P. 2990–2998. DOI: https://doi.org/10.1109/TGRS.2008.921958
18. Mittermayer, J., Moreira, A., Loffeld, O. (1999), "Spotlight SAR Data Processing Using the Frequency Scaling Algorithm", *IEEE Transactions on Geoscience and Remote Sensing*, Vol. 37, No. 5, P. 2198–2214.
19. Mittermayer, J. (2002), "The Frequency Scaling Algorithm and Interferometric Spotlight SAR Processing", *Aerospace Science and Technology*, Vol. 6, No. 2, P. 147–158. DOI: https://doi.org/10.1016/S1270-9638(02)01149-5
20. Guo, Y., Wang, P., Men, Z., Chen, J., Zhou, X., He, T., Cui, L. (2023), "A Modified Range Doppler Algorithm for High-Squint SAR Data Imaging", *Remote Sensing*, Vol. 15, P. 4200. DOI: https://doi.org/10.3390/rs15174200
21. Raney, R. K., Runge, H., Bamler, R., Cumming, I. G., Wong, F. H. (1994), "Precision SAR Processing Using Chirp Scaling", *IEEE Transactions on Geoscience and Remote Sensing*, Vol. 32, No. 4, P. 786–799. DOI: https://doi.org/10.1109/36.298008
22. Jiang, Z., Huang, F., Wan, J., Cheng, Z. (2007), "Modified Frequency Scaling Algorithm for FMCW SAR Data Processing", *Chinese Journal of Aeronautics*, Vol. 20, No. 4, P. 339–345. DOI: https://doi.org/10.1016/S1000-9361(07)60053-3
23. Zheng, J., Cheng, J.-Y., Chen, C.-H. (2008), "A Modified Frequency Scaling Algorithm for Missile-Borne SAR Imaging", *IITA 2008*, Shanghai, China, P. 337–341. DOI: https://doi.org/10.1109/IITA.2008.315

Received (Надійшла) 19.08.2025
Accepted for publication (Прийнята до друку) 07.11.2025
Publication date (Дата публікації) 28.12.2025

About the Authors / Відомості про авторів

Kovalchuk Danyil – PhD, State Scientific and Research Institute of Cybersecurity Technologies and Information Protection, Lead Engineer, Kyiv, Ukraine; e-mail: d.kovalchuk@ws.cip.gov.ua; ORCID ID: https://orcid.org/0009-0007-6847-6610

Zhyla Olha – PhD (Physical and Mathematical Sciences), Kharkiv National University of Radio Electronics, Associate Professor at the Department of Higher Mathematics, Kharkiv, Ukraine; e-mail: olha.kuryzheva@nure.ua; ORCID ID: https://orcid.org/0000-0002-6888-8953

Ковальчук Даниїл Іванович – PhD, Державний науково-дослідний інститут технологій кібербезпеки та захисту інформації, провідний інженер науково-дослідного центру, Київ, Україна.

Жила Ольга Володимирівна – кандидат фізико-математичних наук, Харківський національний університет радіоелектроніки, доцент кафедри вищої математики, Харків, Україна.

ГЕОМЕТРІЯ ВИМІРЮВАНЬ, МОДЕЛІ СИГНАЛІВ І АЛГОРИТМИ ВІДНОВЛЕННЯ РАДІОЗОБРАЖЕНЬ В РАДАРАХ ІЗ СИНТЕЗОВАНОЮ АПЕРТУРОЮ, ЩО ВИКОРИСТОВУЮТЬ БЕЗПЕРЕРВНІ ЛЧМ-СИГНАЛИ

У статті проаналізовано методи формування радіолокаційних зображень поверхні, що отримані за допомогою радара із синтезованою апертурою (РСА) з безперервним зондувальним ЛЧМ-сигналом. Становить інтерес визначення основних алгоритмічних операцій, що виконуються над "сирими" даними після їх реєстрації в приймачах. У роботі розглянуто геометрію вимірювань, зондувальний сигнал і особливості формування "сирих" даних, що визначатимуть подальше оброблення. Для порівняння якості роботи різних алгоритмів запропоновано імітаційну модель формування радіолокаційних зображень в РСА з обробленням безперервних ЛЧМ-сигналів. **Мета дослідження** – створити універсальну геометричну основу для побудови ефективних вимірювальних схем і алгоритмів оброблення сигналів у радіотехнічних системах. **Завдання роботи** передбачають: 1) формалізацію задачі визначення координат за результатами пеленгаційних вимірювань; 2) побудову математичної моделі взаємного розташування об’єктів у тривимірному просторі; 3) визначення впливу геометричних факторів на точність вимірювання; 4) аналіз варіантів одноразового й багаторазового спостереження. **Досягнуті результати** дають змогу встановити аналітичний зв’язок між параметрами вимірювання та конфігурацією просторової сцени, що забезпечує підвищення точності координатного визначення. **Перспективи застосування**: результати можуть бути використані для підвищення ефективності навігаційних, розвідувальних і моніторингових систем, а також у задачах супроводу рухомих об’єктів і побудови систем ситуаційної обізнаності.

Ключові слова: геометрія вимірювань; пеленгація; координатне визначення; тривимірна модель; радіовимірювальна система.

Bibliographic descriptions / Бібліографічні описи

Kovalchuk, D., Zhyla, O. (2025), "Measurement geometry, signal models and agorithms for radio image recovery in synthesized aperture radars using continuous LFM signals", *Management Information Systems and Devises*, No. 4 (187), P. 299–314. DOI: https://doi.org/10.30837/0135-1710.2025.187.299

Ковальчук Д. А., Жила О. В. Геометрія вимірювань, моделі сигналів і алгоритми відновлення радіозображень в радарах із синтезованою апертурою, що використовують безперервні ЛЧМ-сигнали. *Автоматизовані системи управління та прилади автоматики*. 2025. № 4 (187). С. 299–314. DOI: https://doi.org/10.30837/0135-1710.2025.187.299